



Factors Affecting Permeability Reduction of MICP for Fractured Rock

Shuquan Peng¹, Hu Di², Ling Fan^{1*}, Wang Fan² and Liu Qin²

¹ Department of Urban Underground Space Engineering, School of Resources and Safety Engineering, Central South University, Changsha, China, ² School of Resources and Safety Engineering, Central South University, Changsha, China

OPEN ACCESS

Edited by:

Lianyang Zhang,
University of Arizona, United States

Reviewed by:

Kang Peng,
Chongqing University, China
Zhaoyang Xu,
Yangzhou University, China

*Correspondence:

Ling Fan
pqrfanlinger@csu.edu.cn

Specialty section:

This article was submitted to
Earth and Planetary Materials,
a section of the journal
Frontiers in Earth Science

Received: 21 January 2020

Accepted: 25 May 2020

Published: 21 July 2020

Citation:

Peng S, Di H, Fan L, Fan W and
Qin L (2020) Factors Affecting
Permeability Reduction of MICP
for Fractured Rock.
Front. Earth Sci. 8:217.
doi: 10.3389/feart.2020.00217

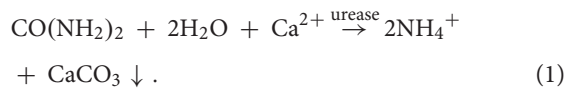
Microbial induced calcite precipitation (MICP) has shown great potential to reduce the permeability of fractured rock, but its permeability reduction characteristic, affected by cementing solution concentration and geometric morphology of fractured rock, has not been presented. In this paper, a self-designed device for experimental MICP grouting and seepage performance was used to study the effects of factors including urea and calcium chloride concentration, fracture roughness and aperture on the permeability reduction of MICP on fractured rock. During the experiment, the same total volume of cement solution was injected into each sample with the same injection times. Based on the experimental results, the Darcy permeability coefficient of MICP grouted fractured rock was reduced to $3\text{--}5 \times 10^{-5}$ m/s by four orders of magnitude smaller than that of non-grouted fractured rock. An increase in fracture roughness, urea and calcium chloride concentrations, as well as a decrease of fracture aperture, caused the MICP grouting ratio in fractured rocks to decrease, as well as a decrease of the Darcy permeability coefficient. In addition, the permeability reduction of MICP on fractured rock increased with the decrement of the above four factors. The permeability coefficient of grouted fractured rock and the permeability reduction of MICP were excessively sensitive to urea concentration. Furthermore, the permeability reduction was fitted well by power function. The research results could provide important guidance and reference significance for MICP grouting application in rock engineering.

Keywords: MICP, grouting, fractured rock, fracture roughness, fracture aperture, permeability coefficient

INTRODUCTION

Microbial induced calcite precipitation (MICP) grouting is a novel bio-grouting technology, and is applied in pollutants fixation, repair of cracks in rock relics, and sealing improvement on underground oil depots and gas reservoirs (Whiffin et al., 2007; Fujita et al., 2008; Ivanov and Chu, 2008; Cunningham et al., 2009, 2011; Dupraz et al., 2009; Mitchell et al., 2009, 2010; De Muynck et al., 2011; Meyer et al., 2011; Chu et al., 2012; Phillips et al., 2013; Zhao et al., 2017a; Peng et al., 2019c, 2020a,d). This technique exhibited some advantages with low grouting pressure, low viscosity, and environmental friendliness, compared with cement-based material grouting and polymer chemical grouting (Lian et al., 2006; Whiffin et al., 2007; Ivanov and Chu, 2008; Mitchell et al., 2013; Phillips et al., 2013; Liu et al., 2019).

The mechanism of MICP grouting was shown as;



The induced-precipitated carbonate calcium cemented and filled the rock fracture, then effectively improved the permeability characteristics of fractured rock (Dejong et al., 2006; De Muynck et al., 2008, 2010; Ivanov and Chu, 2008; Okwadha and Li, 2010; Van Paassen et al., 2010; Cunningham et al., 2014; Zhao et al., 2017b,c, 2019; Peng et al., 2019a,b,c, 2020b,c). For example, the MICP grouting induced the conductivity and permeability reduction of fractured rock surrounding the injection within 3 m by 35 and 99% respectively (Cuthbert et al., 2013). And it also resulted in the seepage velocity reduction of in-suit fractured rock by 25% and the permeability reduction of artificial fractured rock sample up to 80% (Phillips et al., 2016).

The permeability reduction of MICP in fractured rock was affected by grouting rate, grouting times, grouting ratio and fracture aperture, water flowing velocity of the rock. A low grouting rate and multiple-times grouting decreased the permeability coefficient by three orders of magnitude. A fracture aperture of less than 0.7 mm grouted by MICP transformed from Darcy seepage to Non-Darcy (Wu et al., 2019). And the calcium carbonate induced by MICP mainly precipitated in a low flowing velocity zone of the rock fracture, but almost not at all in a high flowing velocity zone (Wu et al., 2018). So the low water flowing velocity benefited the permeability reduction of MICP in fractured rock. Although the concentration of bacterial solution and the geometric morphology of structure plane also theoretically affected the permeability reduction of MICP for fractured rock, these effects were not reported at present.

For this purpose, the effects of fracture aperture, fracture roughness, urea concentration and calcium concentration were experimented on the grouting ratio, permeability coefficient and permeability reduction of MICP grouting in fractured rock. The microstructure and distribution of calcite precipitation on the rock fracture surface were also investigated. Thus the mechanism of permeability reduction of MICP for fractured rock would be presented. These research results could provide a reference in the rock engineering application of MICP.

EXPERIMENTAL MATERIALS AND METHODS

Experimental Solution and Sample

The microbial grouting solution was composed of *Sporosarcina pasteurii* bacteria solution and microbial cementing solution. The *S. pasteurii* was chosen due to its non-pathogenic microorganism with strong survivability such as acid and alkali, high salinity, etc. The *S. pasteurii* strain was inoculated by 5% in a liquid medium and then cultured in a constant temperature shaker at 170 rpm and 30°C for 14 h up to a conductivity of 19 ± 0.5 mM/min and an OD600 of 1.8 ± 0.2 . Thus the *S. pasteurii* bacteria solution was presented. And the liquid cultured medium with was mixed with

1000 ml deionized water, 15.0 g casein peptone, 5.0 g soy peptone, 5.0 g sodium chloride, and 20.0 g urea and was adjusted by NaOH solution up to pH7.3. The microbial cementing solution was a mixed solution of urea and calcium chloride.

The red sandstone samples containing little or no calcium were chosen to decrease the effect of calcium ions in rock on the MICP. Sixteen standard cylindrical red sandstone samples with 50 mm diameter and 100 mm height were split by a Brazilian split-cylinder test. Each split sample was then glued by glue adhesive with a high precise plexiglass pad with a width range from 1.0 to 2.5 mm provided by a laser cutting technique. Thus the single fracture rock samples with apertures of 1.0, 1.5, 2.0, and 2.5 mm were fabricated. Before gluing, the scanned 3D images of fracture surfaces of each sample were gotten by a 3D laser scanner (model LSH400). And based on these 3D images, the absolute average roughness of each sample was calculated by MATLAB software. The fracture roughness and splitting strength of samples were tabulated in **Table 1**. In **Table 1** the fluctuation between the maximum and minimum roughness among samples 1–1 to 1–12 was only 0.023 mm, so the roughness of samples 1–1 to 1–12 are considered the same in this paper. The MICP grouted single fracture rock sample is shown in **Figure 1**.

Experimental Setup

Figure 2 plots the setup of MICP grouting for the fractured rock and seepage experiment. This setup was composed of an MICP grouting device and a seepage experimental device. In **Figure 2A**, the grouting device had two screwed steel columns connecting to a fixing steel plate on the bottom of the fractured rock sample and a moveable one on the top. The rubber grouting pipes with a diameter of 0.3 mm were connected to the sample and the microbial grouting solution by a peristaltic pump. In **Figure 2B**, the plexiglass tube with an inner radius of 26 mm and wall thickness of 3 mm was fixed on the 15 mm thick plywood plate, and had two holes at the height of 200, 500 mm to keep water head constant. The fractured rock grouted by MICP was connected to the plexiglass tube bottom by a heat shrinkable with a diameter of 55 mm to prevent leakages after the occurrence of fractured rock seepage. A beaker was positioned under the sample bottom to collect the seepage effluent.

Experimental Processes

The MICP permeability reduction experiment of single fracture rock was designed to investigate the effect of microbial cementing concentration and fracture geometric morphology. The experimental cases are given in **Table 1**.

Firstly, the single fracture rocks were immersed and saturated for 48 h, and then their permeability coefficients without MICP grouting were tested with the constant-water head of 200 mm using the seepage experiment device shown in **Figure 1B**. The seepage time and seepage volume were recorded by an electronic balance with the sampling frequency of 1 Hz after the seepage was initiated.

Secondly the samples without MICP grouting were dried in a drying box at 70°C for 24 h and then weighed with the electronic balance. Then each dried fractured sample was grouted with 100 ml bacterial solution and 100 ml microbial

TABLE 1 | Experimental cases and parameters of fractured rocks.

Case	Urea concentration/(mol/L)	Calcium chloride concentration/(mol/L)	Fracture aperture ω /mm	Roughness ϵ /mm	Mass		
					Pre-grouting m_0 /g	Post-grouting m_1 /g	$m_1 - m_0$
1-1	0.70	0.90	1.50	0.450	458.83	464.1	5.27
1-2	0.80	0.90	1.50	0.447	462.58	469.26	6.68
1-3	0.90	0.90	1.50	0.453	464.58	471.23	6.65
1-4	1.00	0.90	1.50	0.452	462.02	468.71	6.69
1-5	0.80	0.70	1.50	0.434	465.77	470.47	4.70
1-6	0.80	0.80	1.50	0.452	455.94	461.06	5.12
1-7	0.80	0.90	1.50	0.439	462.58	469.26	6.68
1-8	0.80	1.00	1.50	0.438	463.13	469.78	6.65
1-9	0.80	0.90	1.00	0.432	460.02	465.11	5.09
1-10	0.80	0.90	1.50	0.435	462.58	469.26	6.68
1-11	0.80	0.90	2.00	0.456	464.17	471.34	7.17
1-12	0.80	0.90	2.50	0.429	465.47	473.04	7.57
1-13	0.80	0.90	1.50	0.414	459.54	465.04	5.50
1-14	0.80	0.90	1.50	0.614	460.80	466.87	6.07
1-15	0.80	0.90	1.50	0.673	462.58	468.98	6.40
1-16	0.80	0.90	1.50	0.873	463.13	469.95	6.82

cementing solution from the top of sample fracture to the bottom by the peristaltic pump in 8 doses of 12.5 ml each. And the grouting rate was chosen to be 0.003 mL/s. This is because a too low grouting rate induced easy accumulation of the calcium carbonate precipitation in the grouting port, and hindering the uniform distribution of precipitation on the fracture surface, and a too high grouting rate easily washed away the precipitation. The urea and calcium chloride concentrations of cementing solution were shown in **Table 1**.

After MICP grouting, the fractured samples were placed in a drying box at 70°C for 24 h, and weighed again. The MICP (η) grouting ratio of each fractured rock was calculated by,

$$\eta = \frac{m_1 - m_0}{\rho V} \times 100\% \quad V = AL = \omega DL \quad (2)$$

where m_0 and m_1 is the dry sample mass before and after MICP grouting (g) respectively, and ω is the fracture aperture of the sample (mm). As seen in **Table 1**; ρ is the density of calcium carbonate with a value of 2.71 g/cm³ (Wu et al., 2018); V and A is the volume and the area of longitudinal section of the sample respectively; D and L is the sample diameter and height with a value of 50 and 100 mm, respectively.

Next the dried bio-grouting fractured rock samples were rested at room temperature for 2 days to harden the precipitation of calcium carbonate on the fracture surface of the sample, and successively were immersed and saturated for 48 h. Then the permeability coefficients of single fracture rock samples with MICP grouting were performed with the constant-head of 500 mm by the seepage experiment shown in **Figure 2B**.

Finally about 10 g precipitation was obtained from the bio-grouting fractured rock, and was prepared for scanning electron microscope (SEM). The microscopic morphologies of

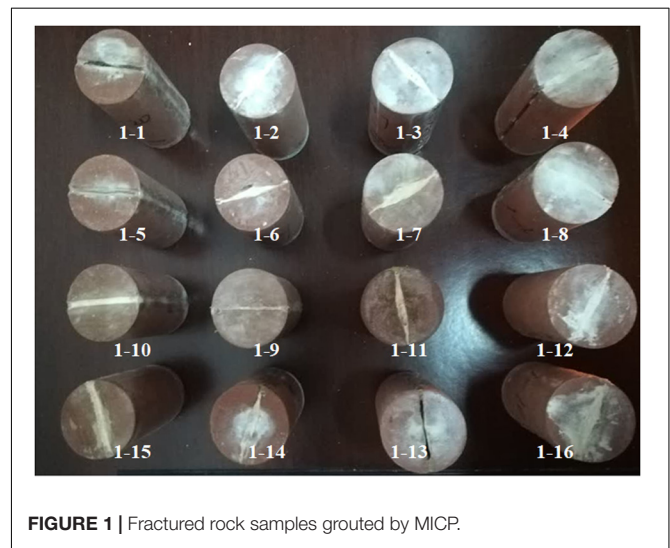


FIGURE 1 | Fractured rock samples grouted by MICP.

the precipitation were scanned by SEM with an energy dispersive spectrometer (EDS) at 20 kV voltages 300 and 5000 times.

RESULTS

Permeability Coefficients

The Darcy permeability coefficient of each fractured rock sample with and without MICP grouting was calculated by:

$$K = \frac{Q\mu L}{A\Delta P}gh \quad A = \omega D. \quad (3)$$

where K is Darcy permeability coefficient, and is denoted as K_a for the fractured rock without MICP grouting and K_b for the

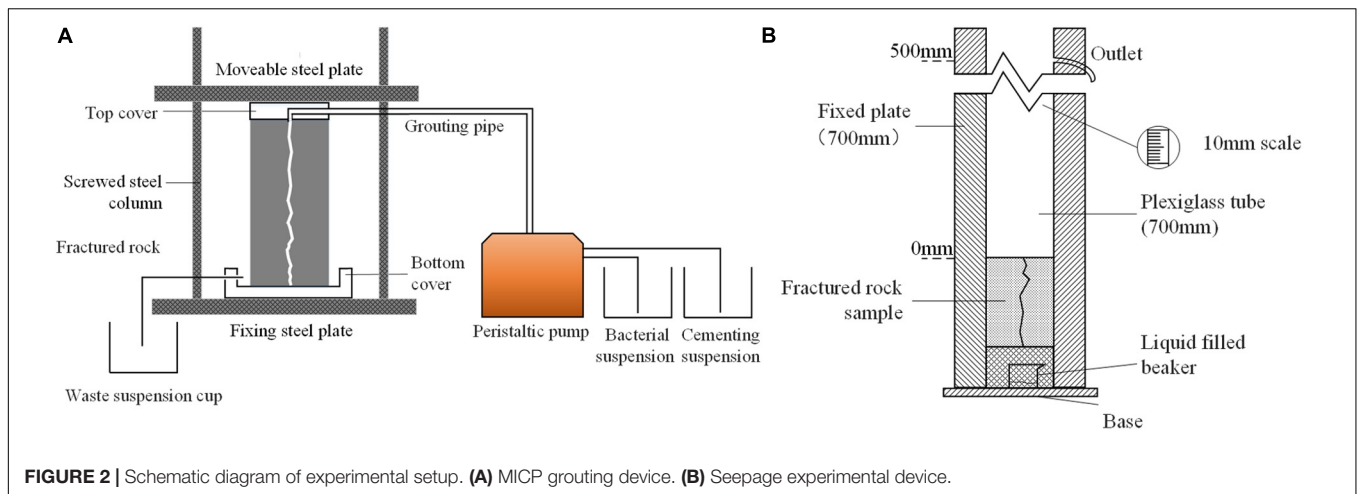


FIGURE 2 | Schematic diagram of experimental setup. **(A)** MICP grouting device. **(B)** Seepage experimental device.

TABLE 2 | Permeability coefficients of fractured rocks.

Case	Factors	A/CM ²	K _a /(M/S)	K _b /(10 ⁻⁴ M/S)	K _b /K _a 10 ⁻⁴
1-1	Urea concentration	0.75	0.2376	0.4693	1.9753
1-2		0.75	0.2443	0.4249	1.7393
1-3		0.75	0.2245	0.3653	1.6272
1-4		0.75	0.2378	0.3600	1.5139
1-5	Calcium chloride concentration	0.75	0.2296	0.4600	2.0035
1-6		0.75	0.2332	0.4380	1.8782
1-7		0.75	0.2543	0.4250	1.6713
1-8		0.75	0.2499	0.4140	1.6567
1-9	Fracture aperture	0.50	0.1536	0.3040	1.9792
1-10		0.75	0.2471	0.4249	1.7196
1-11		1.00	0.3407	0.3707	1.0881
1-12		1.25	0.4342	0.3413	0.7860
1-13	fracture roughness	0.75	0.2295	0.4827	2.1033
1-14		0.75	0.2497	0.4284	1.7157
1-15		0.75	0.2502	0.3973	1.5879
1-16		0.75	0.2344	0.3360	1.4334

one with MICP grouting; Q is the flow rate(m³/s); μ is the dynamic viscosity of water (Pa·S) with value of 1.005×10^{-3} PaS at 20°C; ΔP is the pressure difference between the two ends of the sample. ΔP is equal to 2 kPa before grouting and is equal to 5 kPa after grouting.

Table 2 shows the Darcy permeability coefficients of the single fracture samples with and without MICP grouting. **Table 2** indicated that the permeability coefficients of single fracture rocks after MICP grouting ranged from 0.3040×10^{-4} m/s to 0.4693×10^{-4} m/s, and the ones before MICP grouting from 0.1536 m/s to 0.4342 m/s. The permeability reduction of MICP denoted as K_b/K_a was up to 4 orders of magnitude. Similarly, Cuthbert et al. (2013), Phillips et al. (2016), Tobler et al. (2012), and Wu et al. (2019) experimentally

presented that the permeability reduction was approximately 2–4 orders of magnitude. Therefore it would be inferred that the permeability coefficient of fractured rock was reduced significantly by MICP grouting.

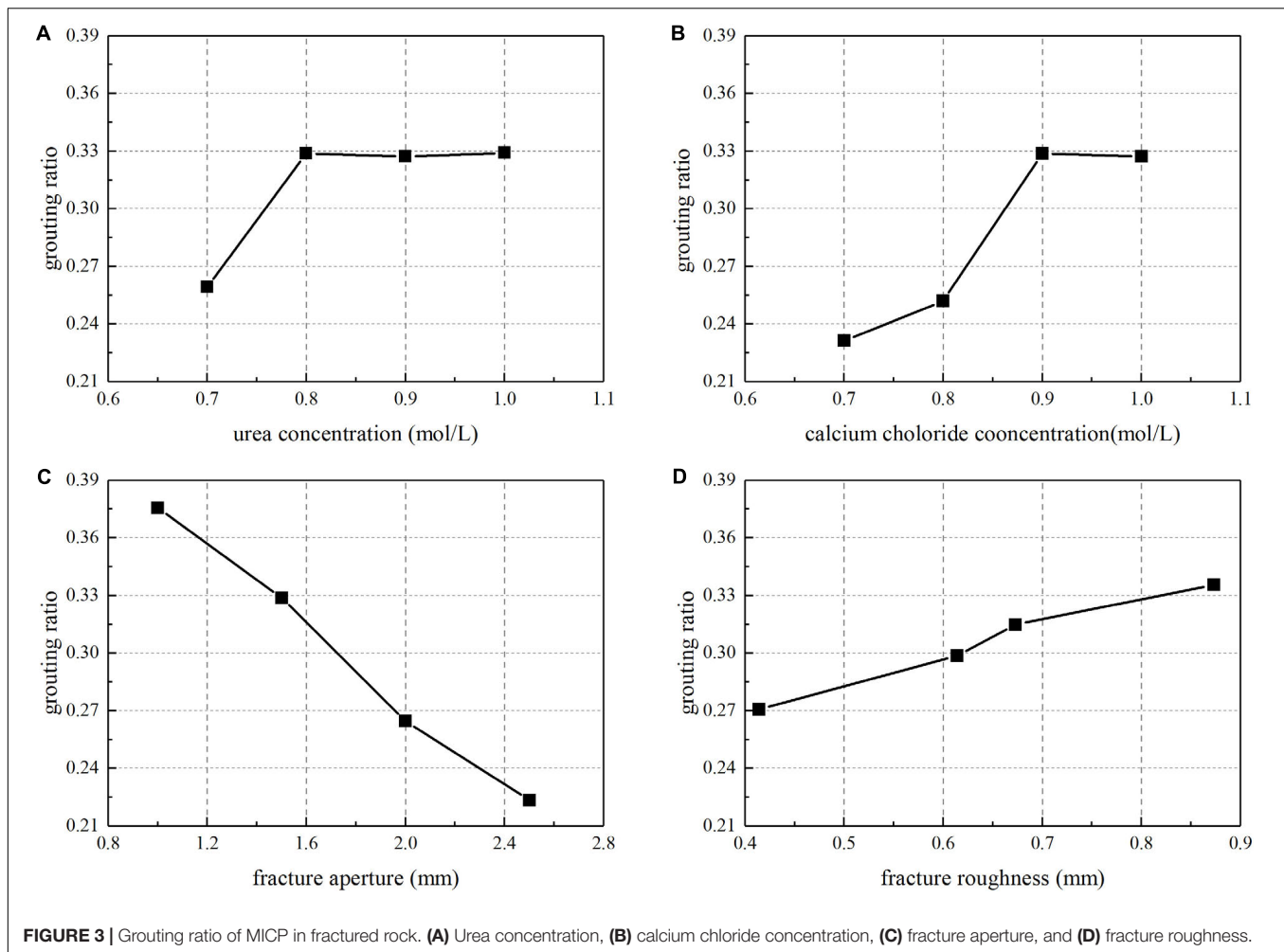
Grouting Ratio

Figure 3 shows the MICP grouting ratio in fractured rock. **Figure 3A,B** indicate that the grouting ratio of MICP increased with increasing urea concentration and calcium chloride concentration, but slightly reduced under the condition of calcium chloride concentration larger than 0.9 mol/L. The reason was that the urease activity was promoted by the increasing of urea concentration, but was inhibited by the calcium chloride concentration larger than 0.9 mol/L (Qian et al., 2009).

It was observed in **Figure 3C** that the grouting ratio of MICP decreased from 37.56 to 22.35%, when the fracture aperture increased from 1.0 to 2.5 mm. The dominant reason was the increasing fracture volume of cases 1–9, 1–10, 1–11, and 1–12. **Figure 3D** also denotes that the MICP grouting ratio increased from 27.06 to 33.55% when fracture roughness increased from 0.414 to 0.873 mm. This was probably because the increase of fracture roughness reduced the flow velocity in fracture for the cases of 1–13, 1–14, 1–15, and 1–16. El Mountassir et al. (2014) suggested that low flow velocity was conducive to the precipitation of calcium carbonate in fracture. So the MICP grouting ratio increased because the increasing fracture roughness increased the production of precipitation on fracture surface.

Permeability K_b

Figure 4 shows the permeability coefficient K_b of fractured samples grouted by MICP. As shown in **Figures 4A,B**, the K_b decreased with the increasing of urea concentration and calcium chloride concentration. Increasing concentration of urea concentration and calcium chloride concentration brought out more calcite precipitation based on Eq. (1). And the increasing precipitation blocked more seepage channels in the fracture when the volume of the fracture was constant for cases 1–1 to 1–8 listed in **Table 1**. Hence



it was deduced that the permeability coefficient decreased with the increasing cementing solution concentration. Moreover, increasing urea concentration promoted bacterial urease activity. And **Figure 4B** also shows that the K_b remained constant when the urea concentration was more than 0.9 mol/L. This agreed with the research results from Nemati and Voordouw (2003).

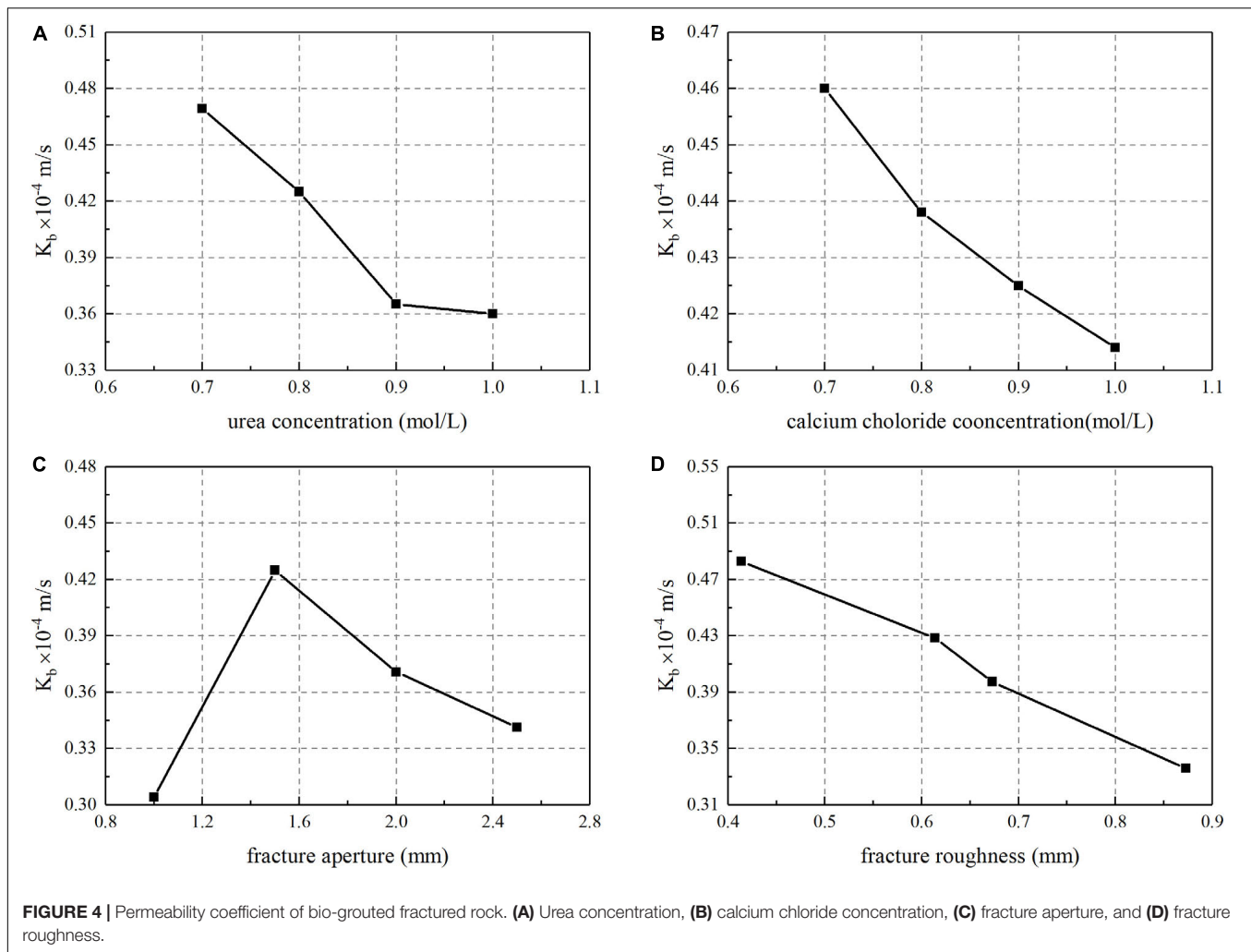
Figure 4C suggested that the permeability coefficient increased with the increasing of the fracture aperture with a range from 1.0 to 1.5 mm, and decreased with the fracture aperture from 1.5 to 2.5 mm. And the similar characteristic of the fracture rock grouted by mortar was reported by Wu et al. (2018, 2019). When the fracture aperture changed, the change of permeability coefficient was obvious. It might be due to the distribution of calcium carbonate precipitation on the fracture with a different aperture. And the non-uniform distribution of calcium carbonate precipitation was detected on the fracture surface of each sample (Stoner et al., 2005; El Mountassir et al., 2014; Minto et al., 2016). What's more, the effect of gravity also affected the permeability characteristics of permeable fractured rock. Under the action of gravity, the MICP precipitation was mostly distributed in

the lower part of the sample. To summarize, the effect of the fracture aperture on the permeability coefficient of fractured rock grouted by MICP was complicated and needed more intensive study.

It can be clearly seen from **Figure 4D** that the larger the fracture roughness, the smaller the permeability coefficient of fractured rock. The existence of fracture roughness formed the low flow velocity zone near to the downstream face of the convex part of the fracture, and the increasing of fracture roughness would form more low flow velocity zones. The low flow velocity zones also facilitated the attachment of calcite precipitation in fracture (El Mountassir et al., 2014). The increasing of attached calcite precipitation would also block the seepage channels in fracture, thus the permeability coefficient of fractured rock grouted by MICP is reduced with increasing fracture roughness.

Permeability Reduction

Figure 5 plotted the permeability reduction of MICP on fractured rock. The smaller the K_b/K_a , the better the permeability reduction. With the increasing of urea concentration, calcium chloride concentration, fracture aperture and roughness, the K_b/K_a decreased, i.e., the permeability reduction



strengthened in **Figure 5**. When the fracture aperture and roughness were generally kept the same, the increase of urea concentration and calcium chloride concentration caused the reduction of the permeability coefficient of MICP-grouted fractured rock (K_b) and the invariability of K_a , hence K_b/K_a diminished. When the concentration of urea and calcium chloride was kept constant, the increasing of fracture roughness obviously reduced K_b and slightly changed K_a listed in **Table 2**, thus K_b/K_a decreased. When the concentration of urea and calcium chloride, and fracture roughness was kept constant, an increase in fracture aperture induced less increment of K_b than the one of K_a , thus K_b/K_a reduced as well.

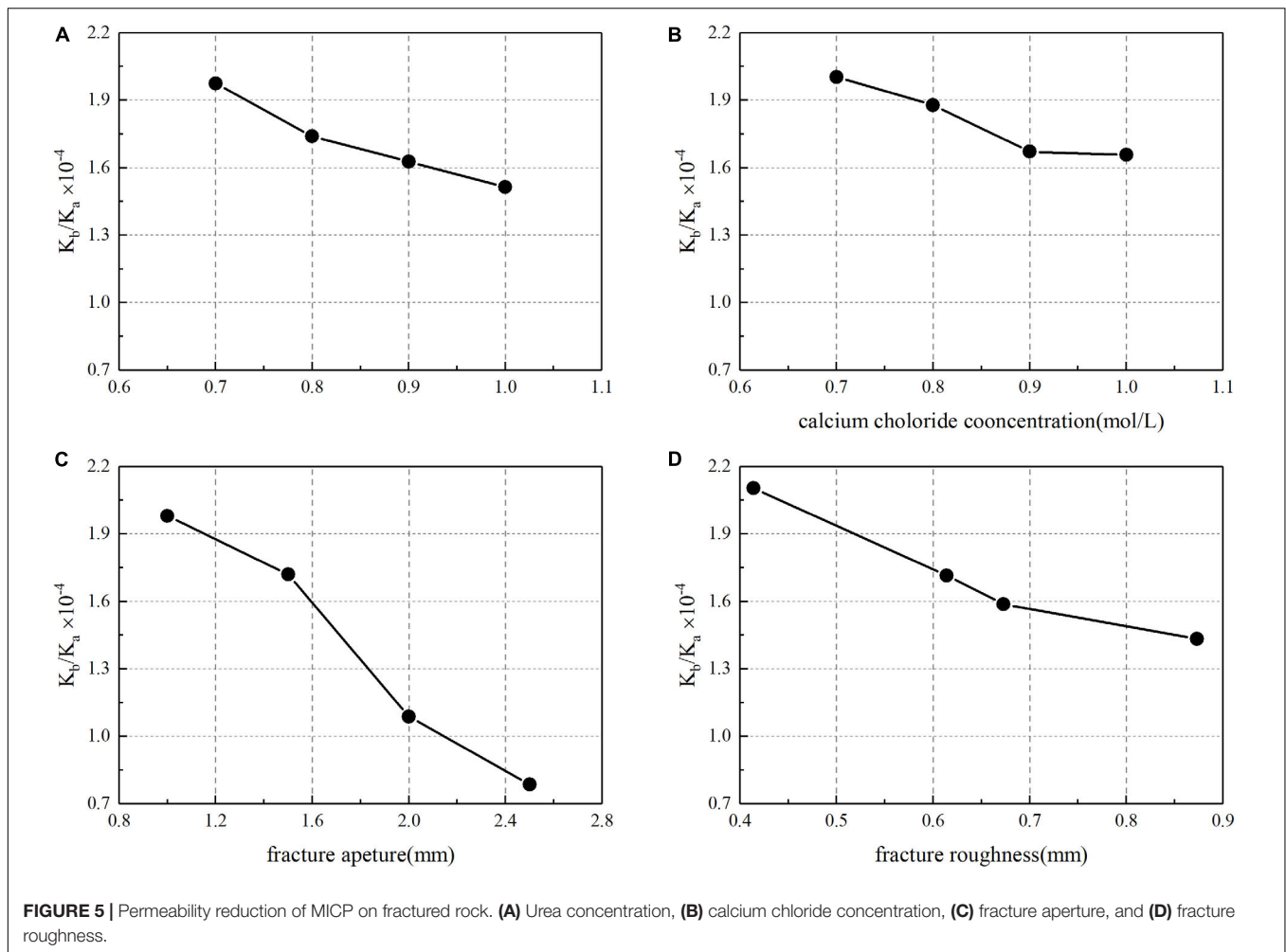
Morphology Analysis of Precipitation

Figure 6 plots the distribution of calcium carbonate on the fracture surface of samples after the seepage experiment. **Figure 6** revealed some white precipitations on the fracture surfaces, which were varied with fracture aperture and roughness. Its SEM characteristic at 300 and 5000 magnifications and X-ray energy spectrum are plotted in **Figure 7**. KCnt in

Figure 7C represents the detected signal strength. **Figure 7** indicates that the particles of precipitation were smooth spheres bonding to each other to form particle clusters and the main component of precipitation was calcium carbonate. These bonding particles might transform the seepage in fractured rock from fracture seepage to uniform pore seepage, which was not easily washed away under the action of hydraulic gradients.

Figure 6A demonstrated that the upper part of fracture had more calcium carbonate deposition than the middle part. This showed that a slight clogging happened at the grouting rate of 0.003 ml/L and gravity. The similar clogging was founded by Stoner et al. (2005), El Mountassir et al. (2014), and Minto et al. (2016). Increasing grouting rate might be a feasible option to diminish the clogging in fractured rock.

Figures 6A,B plotted the possible seepage channels on 1.5 mm and 2.0 mm fracture surfaces while **Figures 6C,D** did not do. It would be deduced that the fractured rock simultaneously generated the fracture seepage and uniform pore seepage in the fracture grouted by MICP.



DISCUSSION

Wu et al. (2019) found that the MICP grouting ratio in the fracture was between 53 and 70%, and Tobler et al. (2016) obtained a range from 30 to 41%, while this paper provided that the one was between 23 and 37%. The reason might be that the difference in the grouting rate and times, as the fracture aperture and roughness caused the variation of the grouting ratio.

Increasing the grouting ratio caused the decreasing of permeability coefficient presented by Wu et al. (2018). In this paper the grouting ratio increased with the increasing of the cementing solution concentration figured in **Figures 3A,B**, when the fracture aperture and roughness did not vary. Therefore the permeability coefficient decreased due to the increasing cementing solution concentration presented in **Figures 4A,B**. And in this paper the grouting ratio also increased with the increasing of the fracture roughness shown in **Figure 3D** when the cementing solution concentration did not change. So the permeability coefficient decreased with increase of fracture roughness shown in **Figure 4D**. In **Figure 3C**, the MICP grouting ratio of fractured rock increased with the decreasing of fracture aperture is shown.

The cubic law of flow in single fracture is amended by Walsh (1981) as

$$\frac{Q}{\Delta P} = C \cdot \frac{1 - \lambda}{1 + \theta \lambda} b_{\max}^3 \quad (4)$$

where C is a constant; θ is an empirical constant. λ is the area contact rate of precipitated calcium carbonate in the fracture and b_{\max} is the maximum aperture of the fracture.

The permeability coefficient is linear to the ratio of Q and ΔP according to Eq. 1. Based on Eq. 4, the permeability coefficient increased, i.e., when λ decreased. λ increased due to the deposition of calcium carbonate in the fractured rock after MICP grouting, but might be weakened by the increasing of the fracture aperture. Hence the permeability reduction of MICP on fractured rock decreased with the increasing of the fracture aperture, as shown in **Figure 5**.

The effect of fracture aperture from 1.0 to 2.5 mm and roughness from 0.4 to 0.9 mm were discussed in this paper, while the effect of fracture aperture larger than 2.5 mm and roughness larger than 0.873 mm need further research.

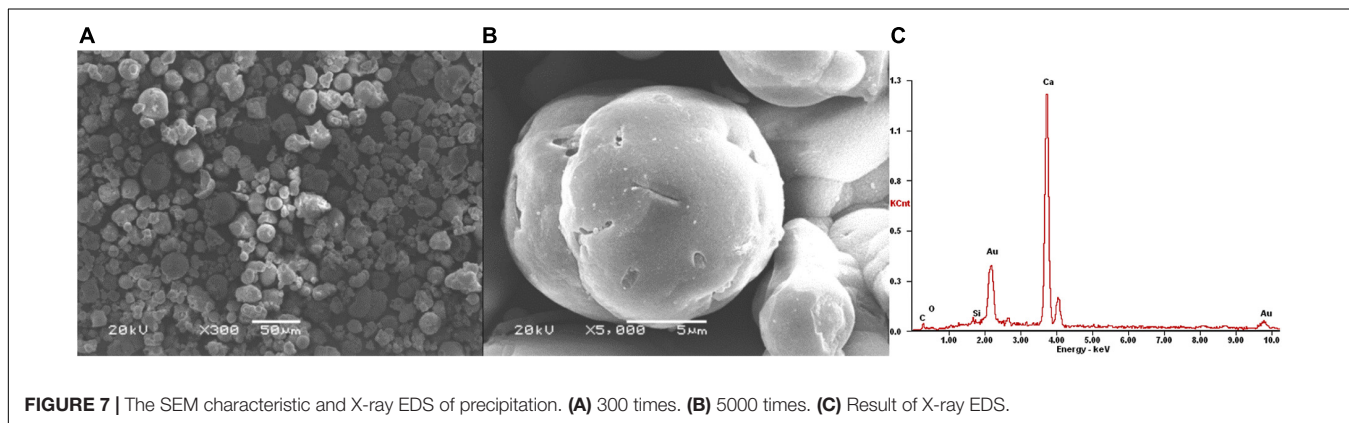
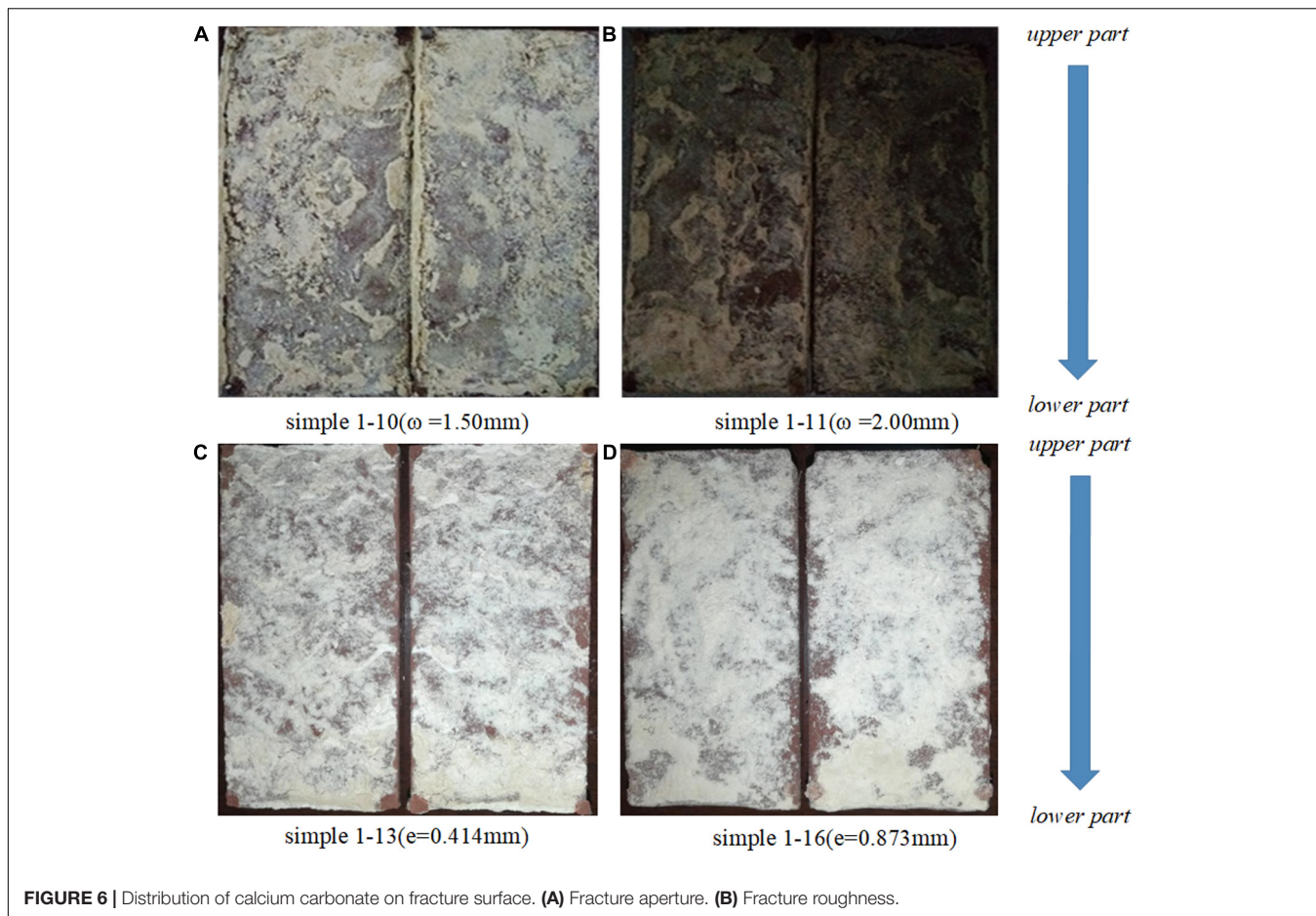
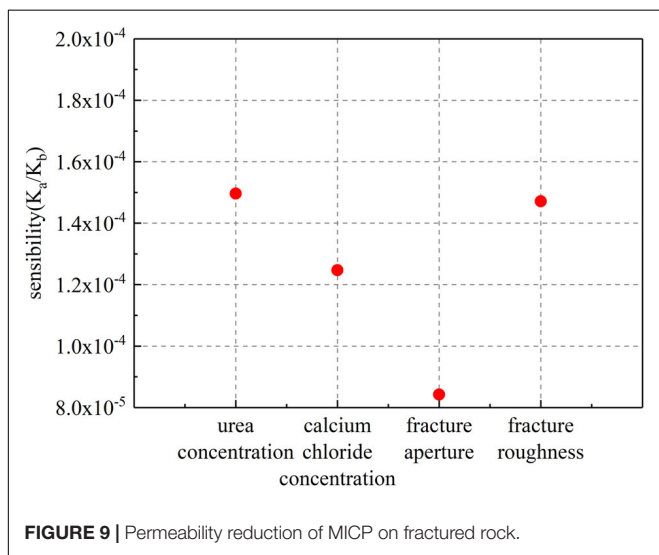
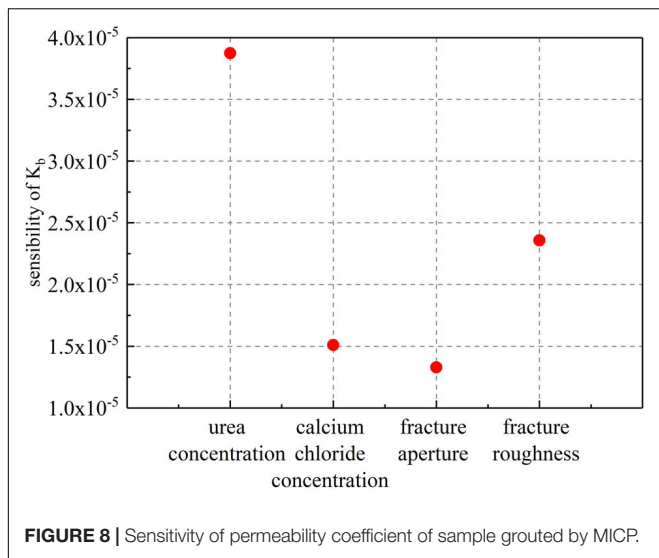


Figure 8 plots the sensitivity of the permeability coefficient of samples grouted by MICP. The sensitivities in **Figure 8** were obtained from the slope of curves in **Figure 4**. It can be found from **Figure 8** that the permeability coefficient was the most sensitive to urea concentration among the four factors in this paper. Therefore it was concluded that the increasing of urea concentration should be firstly selected to reduce the permeability coefficient of fractured rock besides multiple-times grouting.

Figure 9 plots the sensitivity of permeability reduction of MICP in fractured rock. The sensitivities in **Figure 9** were obtained from the slope of curves in **Figure 5**. **Figure 9** indicated that the permeability reduction was more sensitive to urea concentration, fracture roughness and calcium chloride concentration than fracture aperture. Therefore it was concluded that the MICP grouting was suitable for fractured rock with different apertures.



Considering urea concentration, calcium chloride concentration, fracture aperture and fracture roughness as independent variables, K_b/K_a was fitted by power function using the least square method. Then we could get:

$$\frac{K_b}{K_a} = 1.615 \times 10^{-4} x_1^{-0.659} x_2^{-0.671} x_3^{-0.786} x_4^{-0.176} (R = 0.832) \tag{5}$$

where $x_1, x_2, x_3,$ and x_4 is urea concentration, calcium chloride concentration, fracture aperture and fracture roughness respectively.

From Eq. 5, the permeability reduction was well fitted by power function of concentration, calcium chloride concentration, fracture aperture and fracture roughness with a correlation coefficient of 0.832.

It should be pointed out that this research was mainly based on laboratory experiments, and no in-depth analysis was made in terms of the injection rate.

Although the MICP grouting technology significantly reduced the permeability of fractured rock sample, the permeability coefficient of MICP grouted fractured rock was still larger than 5×10^{-7} m/s approximately corresponding to 5 Lu that was the critical value of anti-seepage grouting standards for fractured rock in tunnels, subways, and dams.

CONCLUSION

In this paper, the MICP grouting fractured rock seepage experiment was performed to study the effects of MICP on permeability characteristics of single fracture rock considering fracture geometric morphology and microbial cementing solution concentration. The conclusions are as follows:

- (1) MICP grouting reduced the Darcy permeability coefficient of fractured rock to $3-5 \times 10^{-5}$ m/s by four orders of magnitude compared with that of non-grouted fractured rock.
- (2) The MICP grouting ratio of fractured rock increased when increasing the fracture roughness, urea and calcium chloride concentrations and decreasing of fracture aperture.
- (3) The Darcy permeability coefficient of fractured rock grouted by MICP increased with the decreasing of fracture roughness, urea and calcium chloride concentrations and increasing of fracture aperture, and was the most sensitive to urea concentration.
- (4) The permeability reduction of MICP on fractured rock increased with the decreasing of fracture roughness, urea and calcium chloride concentrations and with the increasing of the fracture aperture, and was well fitted by power function.

DATA AVAILABILITY STATEMENT

The raw data supporting the conclusions of this article will be made available by the authors, without undue reservation, to any qualified researcher.

AUTHOR CONTRIBUTIONS

SP, HD, and LF conceived of the study together. SP and HD designed and carried out the analysis, and wrote the manuscript with contributions and input from WF and LQ. All authors contributed to the discussion.

FUNDING

This project was supported by the Natural Science Foundation of China (Grant # 51674287, #51874354, and #51508579).

REFERENCES

- Chu, J., Stabnikov, V., and Ivanov, V. (2012). Microbially induced calcium carbonate precipitation on surface or in the bulk of soil. *Geomicrobiol. J.* 29, 544–549. doi: 10.1080/01490451.2011.592929
- Cunningham, A. B., Gerlach, R., Spangler, L., and Mitchell, A. C. (2009). “Microbially enhanced geologic containment of sequestered supercritical CO₂,” in *Proceedings of the 9th International Conference on Greenhouse Gas Control Technologies (GHGT-9)*, eds J. Gale, H. Herzog, and J. Braitsch (Washington DC: Elsevier), 3245–3252. doi: 10.1016/j.egypro.2009.02.109
- Cunningham, A. B., Gerlach, R., Spangler, L., Mitchell, A. C., Parks, S., and Phillips, A. (2011). “Reducing the risk of well bore leakage of CO₂ using engineered biomineralization barriers,” in *Proceedings of the 10th International Conference on Greenhouse Gas Control Technologies*, eds J. Gale, C. Hendriks, and W. Turkenberg (Washington DC: Elsevier), 5178–5185. doi: 10.1016/j.egypro.2011.02.495
- Cunningham, A. B., Phillips, A. J., Troyer, E., Lauchnor, E., Hiebert, R., Gerlach, R., et al. (2014). Wellbore leakage mitigation using engineered biomineralization. 12th International Conference on Greenhouse Gas Control Technologies. *Ghgt* 3, 4612–4619. doi: 10.1016/j.egypro.2014.11.494
- Cuthbert, M. O., Mcmillan, L. A., Handley-Sidhu, S., Riley, M. S., Tobler, D. J., and Phoenix, V. R. (2013). A field and modeling study of fractured rock permeability reduction using microbially induced calcite precipitation. *Environ. Sci. Technol.* 47, 13637–13643.
- De Muynck, W., Debrouwer, D., De Belie, N., and Verstraete, W. (2008). Bacterial carbonate precipitation improves the durability of cementitious materials. *Cem. Concr. Res.* 38, 1005–1014. doi: 10.1016/j.cemconres.2008.03.005
- De Muynck, W., Leuridan, S., Van Loo, D., Verbeken, K., Cnudde, V., De Belie, N., et al. (2011). Influence of pore structure on the effectiveness of a biogenic carbonate surface treatment for limestone conservation. *Appl. Environ. Microbiol.* 77, 6808–6820. doi: 10.1016/j.ecoleng.2009.03.025
- De Muynck, W., Verbeken, K., De Belie, N., and Verstraete, W. (2010). Influence of urea and calcium dosage on the effectiveness of bacterially induced carbonate precipitation on limestone. *Ecol. Eng.* 36, 99–111. doi: 10.1016/j.ecoleng.2009.03.025
- Dejong, J. T., Fritzges, M. B., and Nusslein, K. (2006). Microbially induced cementation to control sand response to undrained shear. *J. Geotech. Geoenviron. Eng.* 132, 1381–1392. doi: 10.1061/(ASCE)1090-02412006132:111381
- Dupraz, S., Menez, B., Gouze, P., Leprovost, R., Benezeth, P., Pokrovsky, O. S., et al. (2009). Experimental approach of CO₂ biomineralization in deep saline aquifers. *Chem. Geol.* 265, 54–62. doi: 10.1016/j.chemgeo.2008.12.012
- El Mountassir, G., Lunn, R. J., Moir, H., and Maclachlan, E. (2014). Hydrodynamic coupling in microbially mediated fracture mineralization: formation of self-organized groundwater flow channels. *Water Resour. Res.* 50, 1–16. doi: 10.1002/2013WR013578
- Fujita, Y., Taylor, J. L., Gresham, T. L. T., Delwiche, M. E., Colwell, F. S., McIning, T. L., et al. (2008). Stimulation of microbial urea hydrolysis in groundwater to enhance calcite precipitation. *Environ. Sci. Technol.* 42, 3025–3032. doi: 10.1021/es702643g
- Ivanov, V., and Chu, J. (2008). Applications of microorganisms to geotechnical engineering for biologging and biocementation of soil in situ. *Rev. Environ. Sci. Biotechnol.* 7, 139–153. doi: 10.1007/s11157-007-9126-3
- Lian, B., Hu, Q., Chen, J., Ji, J., and Teng, H. H. (2006). Carbonate biomineralization induced by soil bacterium *Bacillus megaterium*. *Geochim. Cosmochim. Acta* 70, 5522–5535. doi: 10.1016/j.gca.2006.08.044
- Liu, K., Li, X., Hao, H., Li, X., Sha, Y., Wang, W., et al. (2019). Study on the raising technique using one blast based on the combination of long-hole presplitting and vertical crater retreat multiple-deck shots. *Int. J. Rock Mech. Min. Sci.* 113, 41–58. doi: 10.1016/j.ijrmm.2018.11.012
- Meyer, F. D., Bang, S., Min, S., Stetler, L., and Bang, S. (2011). Microbiologically-induced soil stabilization: application of *Sporosarcina pasteurii* for fugitive dust control. *Geotech. Special Publ.* 4002–4011. doi: 10.1061/41165(397)409
- Minto, J. M., Maclachlan, E., El Mountassir, G., and Lunn, R. J. (2016). Rock fracture grouting with microbially induced carbonate precipitation. *Water Resour. Res.* 52, 8810–8827. doi: 10.1002/2016WR018884
- Mitchell, A. C., Dideriksen, K., Spangler, L. H., Cunningham, A. B., and Gerlach, R. (2010). Microbially Enhanced Carbon Capture and Storage by Mineral-Trapping and Solubility-Trapping. *Environ. Sci. Technol.* 44, 5270–5276. doi: 10.1021/es903270w
- Mitchell, A. C., Phillips, A., Schultz, L., Parks, S., Spangler, L., Cunningham, A. B., et al. (2013). Microbial CaCO₃ mineral formation and stability in an experimentally simulated high pressure saline aquifer with supercritical CO₂. *Int. J. Greenhouse Gas Control* 15, 86–96. doi: 10.1016/j.ijggc.2013.02.001
- Mitchell, A. C., Phillips, A. J., Hiebert, R., Gerlach, R., Spangler, L. H., and Cunningham, A. B. (2009). Biofilm enhanced geologic sequestration of supercritical CO₂. *Int. J. Greenhouse Gas Control* 3, 90–99. doi: 10.1016/j.ijggc.2008.05.002
- Nemati, M., and Voordouw, G. (2003). Modification of porous media permeability, using calcium carbonate produced enzymatically in situ. *Enzyme Microb. Technol.* 33, 635–642. doi: 10.1016/S0141-0229(03)00191-1
- Okwadha, G. D. O., and Li, J. (2010). Optimum conditions for microbial carbonate precipitation. *Chemosphere* 81, 1143–1148. doi: 10.1016/j.chemosphere.2010.09.066
- Peng, K., Liu, Z., Zou, Q., Wu, Q., and Zhou, J. (2020a). Mechanical property of granite from different buried depths under uniaxial compression and dynamic impact: an energy-based investigation. *Powder Technol.* 362, 729–744. doi: 10.1016/j.powtec.2019.11.101
- Peng, K., Lv, H., Yan, F., Zou, Q., Song, X., and Liu, Z. (2020b). Effects of temperature on mechanical properties of granite under different fracture modes. *Eng. Fract. Mech.* 226:106838. doi: 10.1016/j.engfractmech.2019.106838
- Peng, K., Shi, S., Zou, Q., Zhang, Y., and Tan, G. (2020c). Gas permeability characteristics and energy evolution laws of gas-bearing coal under multi-level stress paths. *Nat. Resour. Res.* 1–2. doi: 10.1007/s11053-020-09636-0
- Peng, K., Zhou, J., Zou, Q., and Song, X. (2020d). Effect of loading frequency on the deformation behaviours of sandstones subjected to cyclic loads and its underlying mechanism. *Int. J. Fatigue* 131:105349. doi: 10.1016/j.ijfatigue.2019.105349
- Peng, K., Wang, Y., Zou, Q., Liu, Z., and Mou, J. (2019a). Effect of crack angles on energy characteristics of sandstones under a complex stress path. *Eng. Fract. Mech.* 218:106577. doi: 10.1016/j.engfractmech.2019.106577
- Peng, K., Zhou, J., Zou, Q., and Yan, F. (2019b). Deformation characteristics of sandstones during cyclic loading and unloading with varying lower limits of stress under different confining pressures. *Int. J. Fatigue* 127, 82–100. doi: 10.1016/j.ijfatigue.2019.06.007
- Peng, S., Wang, F., Li, X., Fan, L., and Gong, F. (2019c). A microbial method for improving salt swelling behavior of sulfate saline soil by an experimental study. *Alexandria Eng. J.* 58, 1353–1366. doi: 10.1016/j.aej.2019.11.006
- Phillips, A. J., Cunningham, A. B., Gerlach, R., Hiebert, R., Hwang, C., Lomans, B. P., et al. (2016). Fracture sealing with microbially-induced calcium carbonate precipitation: a field study. *Environ. Sci. Technol.* 50, 4111–4117. doi: 10.1021/acs.est.5b05559
- Phillips, A. J., Gerlach, R., Lauchnor, E., Mitchell, A. C., Cunningham, A. B., and Spangler, L. (2013). Engineered applications of ureolytic biomineralization: a review. *Biofouling* 29, 715–733. doi: 10.1080/08927014.2013.796550
- Qian, C. X., Wang, J. Y., Wang, R. X., and Cheng, L. (2009). Corrosion protection of cement-based building materials by surface deposition of CaCO₃ by *Bacillus pasteurii*. *Mater. Sci. Eng. C* 29, 1273–1280. doi: 10.1016/j.msec.2008.10.025
- Stoner, D. L., Watson, S. M., Stedtfeld, R. D., Meakin, P., Griffel, L. K., Tyler, T. L., et al. (2005). Application of stereolithographic custom models for studying the impact of biofilms and mineral precipitation on fluid flow. *Appl. Environ. Microbiol.* 71, 8721–8728. doi: 10.1128/AEM.71.12.8721-8728.2005
- Tobler, D. J., Blanco, J. D. R., Sorensen, H. O., Stipp, S. L. S., and Dideriksen, K. (2016). Effect of pH on amorphous calcium carbonate structure and transformation. *Cryst. Growth Des.* 16, 4500–4508. doi: 10.1021/acs.cgd.6b00630
- Tobler, D. J., Maclachlan, E., and Phoenix, V. R. (2012). Microbially mediated plugging of porous media and the impact of differing injection strategies. *Ecol. Eng.* 42, 270–278. doi: 10.1016/j.ecoleng.2012.02.027
- Van Paassen, L. A., Ghose, R., Van Der Linden, T. J. M., Van Der Star, W. R. L., and Van Loosdrecht, M. C. M. (2010). Quantifying biomediated ground improvement by ureolysis: large-scale biogROUT experiment. *J. Geotech. Geoenviron. Eng.* 136, 1721–1728. doi: 10.1061/(ASCE)GT.1943-5606.0000382
- Walsh, J. B. (1981). Effect of pore pressure and confining pressure on fracture permeability. *Int. J. Rock. Mech. Min. Sci. Geomech.* 19:A6. doi: 10.1016/0148-9062(82)90760-4
- Whiffin, V. S., Van Paassen, L. A., and Harkes, M. P. (2007). Microbial carbonate precipitation as a soil improvement technique. *Geomicrobiol. J.* 24, 417–423. doi: 10.1080/01490450701436505

- Wu, C., Chu, J., Wu, S., and Guo, W. (2018). Quantifying the permeability reduction of biogROUTED rock fracture. *Rock Mech. Rock Eng.* 52, 947–954. doi: 10.1007/s00603-018-1669-9
- Wu, C., Chu, J., Wu, S., and Hong, Y. (2019). 3D characterization of microbially induced carbonate precipitation in rock fracture and the resulted permeability reduction. *Eng. Geol.* 249, 23–30. doi: 10.1016/j.enggeo.2018.12.017
- Zhao, Y., Tang, J., Chen, Y., Zhang, L., Wang, W., Wan, W., et al. (2017a). Hydromechanical coupling experiments for mechanical and permeability characteristics of fractured limestone in complete stress–strain process. *Environ. Earth* 76:24. doi: 10.1007/s12665-016-6322-x
- Zhao, Y., Zhang, L., Wang, W., Tang, J., Lin, H., and Wan, W. (2017b). Transient pulse experiment and morphological analysis of single rock fractures. *Int. J. Rock Mech. Min. Sci.* 91, 139–154. doi: 10.1016/j.ijrmms.2016.11.016
- Zhao, Y. L., Wang, Y. X., Wang, W. J., Wan, W., and Tang, J. Z. (2017c). Modeling of non-linear rheological behavior of hard rock using triaxial rheological experiment. *Int. J. Rock Mech. Min. Sci.* 93, 66–75. doi: 10.1016/j.ijrmms.2017.01.004
- Zhao, Y., Wang, Y., Wang, W., Tang, L., Liu, Q., and Cheng, G. (2019). Modeling of rheological fracture behavior of rock cracks subjected to hydraulic pressure and far field stresses. *Theor. Appl. Fract. Mech.* 101, 59–66. doi: 10.1016/j.tafmec.2019.01.026

Conflict of Interest: The authors declare that the research was conducted in the absence of any commercial or financial relationships that could be construed as a potential conflict of interest.

Copyright © 2020 Peng, Di, Fan, Fan and Qin. This is an open-access article distributed under the terms of the Creative Commons Attribution License (CC BY). The use, distribution or reproduction in other forums is permitted, provided the original author(s) and the copyright owner(s) are credited and that the original publication in this journal is cited, in accordance with accepted academic practice. No use, distribution or reproduction is permitted which does not comply with these terms.